



Article

Effect of Corona Treatment Method to Carvacrol Nanocoating Process for Carvacrol/Halloysite-Nanotube/Low-Density-Polyethylene Active Packaging Films Development

Aris E. Giannakas ^{1,*}, Vassilios K. Karabagias ¹, Amarildo Ndreka ¹, Aikaterini Dimitrakou ², Areti A. Leontiou ¹, Katerina Katerinopoulou ¹, Michael A. Karakassides ², Charalampos Proestos ³ and Constantinou E. Salmas ^{2,*}

¹ Department of Food Science and Technology, University of Patras, 30100 Agrinio, Greece; vkarampagias@upatras.gr (V.K.K.); amarildondreka5@gmail.com (A.N.); aleontiu@upatras.gr (A.A.L.); akaterin@upatras.gr (K.K.)

² Department of Material Science and Engineering, University of Ioannina, 45110 Ioannina, Greece; a.dimitrakou@uoi.gr (A.D.); mkarakas@uoi.gr (M.A.K.)

³ Laboratory of Food Chemistry, Department of Chemistry, National and Kapodistrian University of Athens Zografou, 15771 Athens, Greece; harpro@chem.uoa.gr

* Correspondence: agiannakas@upatras.gr (A.E.G.); ksalmas@uoi.gr (C.E.S.)

Abstract: Active food packaging incorporated with natural plant extracts as food preservatives, which will totally replace chemical preservatives gradually, are of major interest. Sequentially to our and other scientists' previous work, in this paper we present the results of a study on the development of a novel active food packaging film based on the incorporation of a natural-halloysite/carcvacrol-extract nanohybrid with the commercially used low-density polyethylene. The corona-treatment procedure was employed to incorporate a natural preservative on to the optimum final film. Packaging films are formatted with and without incorporation of natural-halloysite/carcvacrol-extract nanohybrid and are coated externally, directly or via corona-treatment, with carvacrol essential oil. Mechanical, physicochemical, and preservation tests indicated that the low-density polyethylene incorporated perfectly with a natural-halloysite/carcvacrol-extract nanohybrid. The extra external coating of the film with pure carvacrol extract using the corona-treatment technique led to approximately 100% higher Young Modulus values, slightly decreased ultimate strength by 20%, and exhibited almost stable elongation at break properties. The water vapor and oxygen properties were increased by 45 and 43%, correspondingly, compared to those of pure low-density polyethylene film. Finally, the antioxidant activity of the corona-treated film increased by 28% compared to the untreated film coated with carvacrol because of the controlled release rate of the carvacrol.

Keywords: low-density polyethylene; carvacrol; halloysite nanotube; corona treatment; nanocoating; active packaging; control release



Citation: Giannakas, A.E.; Karabagias, V.K.; Ndreka, A.; Dimitrakou, A.; Leontiou, A.A.; Katerinopoulou, K.; Karakassides, M.A.; Proestos, C.; Salmas, C.E. Effect of Corona Treatment Method to Carvacrol Nanocoating Process for Carvacrol/Halloysite-Nanotube/Low-Density-Polyethylene Active Packaging Films Development. *Nanomanufacturing* **2024**, *4*, 138–158. <https://doi.org/10.3390/nanomanufacturing4030010>

Academic Editor: Candido Fabrizio Pirri

Received: 24 May 2024

Revised: 5 July 2024

Accepted: 10 July 2024

Published: 22 July 2024



Copyright: © 2024 by the authors. Licensee MDPI, Basel, Switzerland. This article is an open access article distributed under the terms and conditions of the Creative Commons Attribution (CC BY) license (<https://creativecommons.org/licenses/by/4.0/>).

1. Introduction

In the last few years, bioeconomy and sustainability trends are affecting all the scientific fields of research and development. In the Food Technology and Food Packaging sector there is a trend of replacing chemical additives and preservatives such as butylated hydroxyanisole (BHA) and butylated hydroxytoluene (BHT) with bioactive compounds such as natural extracts and essential oils (EOs) [1–3]. In this direction, EOs have extensively been studied as antioxidant and antibacterial agents in active packaging systems [4–6]. EOs are biologically active compounds, which are volatile in nature, safe, environmentally friendly, and have good consumer acceptance as they are categorized as generally recognized as safe (GRAS) by the United States Food and Drug Administration (USFDA). EOs extracted from plants were found to have a good potential to inhibit growth of common bacteria

associated with food spoilage. Typical examples of such compounds are thyme, cloves, cinnamon, tea tree, mint, oregano, lemongrass, citronella, etc. In the literature, there is a plethora of studies with essential oils (EOs) addition into polymers such as polyethylene (PE), low-density polyethylene [7–9], polyethylene terephthalate (PET) [10], polystyrene (PS) [11] and biopolymers such as starch, chitosan, gelatin, alginates, and poly-lactide acid (PLA) active packaging films [12–20]. In addition, there are many studies that feature the use of EOs active components in active packaging systems such as limonene, eugenol, thymol, cinnamaldehyde, and carvacrol [21–28]. Carvacrol (CV) is a phenolic monoterpene found in EOs of oregano (*Origanum vulgare*), thyme (*Thymus vulgaris*), pepperwort (*Lepidium flavum*), wild bergamot (*Citrus aurantium bergamia*), and other plants and is useful for its significant antibacterial, antifungal, antimicrobial, and antioxidant activities [29,30]. Thymol (TO) shares a similar chemical formula with CV; they are structural isomers. The only difference in the chemical structure of carvacrol and thymol is that the former contains a hydroxyl group in the ortho position of the benzene ring while the latter has its hydroxyl group in the meta position. Carvacrol exhibits high antimicrobial activity compared to other volatile compounds present in EOs. This can be attributed to the presence of the free hydroxyl group, hydrophobicity, and reactivity of their phenol moiety [31].

In the last decade, many technologies have been employed for incorporating EOs and their derivatives in active food packaging films. Because of EOs' volatile nature, the direct incorporation in the packaging film caused their quick loss, so technologies such as the adsorption on nanocarriers, e.g., nanoclays, natural zeolite, activated carbon, and silicas, as well as electrospinning, have been proposed and studied in the literature [32–37]. In addition, antibacterial coatings in packaging films are a rising topic in the field of active packaging materials [38–41]. The development of such antibacterial coatings implies the use of novel surface treatment methods such as chemical surface, UV, corona, and plasma [42]. Among them, corona treatment can activate polymeric surfaces to facilitate the adhesion of various functional coatings, while the possibility of creating specialized antimicrobial coatings with natural extracts and EOs can further be based on this method [43–45].

In recent reports, our research group has developed the technology of incorporating EOs and their components into nanostructures such as nanoclays, natural zeolite, and activated carbon for the development of innovative active packaging films, pads, and coating that succeeds in increasing the shelf life of dairy, fruit, and meat products [46–51]. In this paper, a study of the development of antibacterial nanocoatings of CV on the surface of low-density polyethylene (LDPE) films is reported for the first time. LDPE was chosen as one of the most extensively used packaging materials due to its flexibility and good water barrier properties. As “blank” samples, a pure LDPE sample, an LDPE sample reinforced with a halloysite nanotube (HNT) nanoclay (LDPE/HNT), and a LDPE sample reinforced with a halloysite nanotube (HNT) nanoclay modified with CV (LDPE/CV@HNT) were collected. These three starting materials were surface modified with a CV nanocoating without treatment and after a corona treatment process. The innovative points of the current study which were for the first time reported are (i) the application of CV as a nanocoating to develop active packaging materials by using novel packaging technologies such as corona treatment, (ii) the application of CV as a nanocoating with corona treatment process not only in pure polymeric matrix such as pure LDPE but also in LDPE/HNT and LDPE/CV@HNT nanocomposite active films, (iii) a comparison study via physicochemical characterization and packaging properties characterization between active packaging materials coated with CV via corona treatment method and active packaging materials coated with CV without corona treatment, and (iv) the effect of HNT and CV@HNT on the effectiveness of CV nanocoating. The overall study provides new perspectives for the application of processes already used in food packaging such as printing ink technologies and packaging surface activation technologies in the utilization of EOs and their derivatives as antioxidant/antimicrobial nanocoatings of food packaging materials.

2. Materials and Methods

2.1. Materials

Carvacrol (CV) with a CAS no: 499-75-2, halloysite nanotubes (HNT) with a CAS. No. 1332-58-7, LDPE with a CAS no. of 9002-88-4 and extra pure DiPhenyl-1-PicrylHydrazyl (DPPH) with CAS no. of 1898-66-4 were supplied by Sigma-Aldrich (Sigma-Aldrich, St. Louis, MO, USA). Thiobarbituric acid (TBA) pro-analyze was purchased from Merck KGaA, 64271 Darmstadt, Germany. Acetone 99% for analysis was supplied by Fisher Scientific, Bishop Meadow Road, Loughborough LE11 SRG, UK.

2.2. Preparation of CV@HNT Nanohybrid

A total of 3 g of HNT were dried at 120 °C under vacuum. Then, in the dried HNT, approximately 5 mL of CV was added drop by drop and stirred (300 rpm) until a slurry was obtained. The obtained slurry was then stirred overnight since the excess of CV evaporated. The obtained CV@HNT nanohybrid powder was stored for further use.

2.3. Preparation of “Blank” LDPE, LDPE/HNT, and LDPE/CV@HNT Films

The development of LDPE, LDPE/HNT, and LDPE/CV@HNT films was accomplished by employing a Mini Lab twin-screw extruder (Haake Mini Lab II, Thermo Scientific, ANTISEL, S.A., Athens, Greece) operated at 140 °C and 100 rpm for 3 min. For pure LDPE film, 5 g of LDPE pellets were blended. For the LDPE/HNT and LDPE/CV@HNT films, 4.5 g of LDPE pellets were mixed with 0.5 g of pure HNT and 0.5 g of modified CV@HNT powders to obtain composites with 10 wt.% HNT and CV@HNT content, correspondingly, according to the recent publication [47]. The obtained composites were transformed into films (see Figure 1) by using a hydraulic press with heated platens and heat-pressing. Approximately 1.0 g pellets at 110 °C and a constant pressure of 2 MPa were used to obtain films with 11 cm diameter and an average thickness of 0.06–0.12 mm.

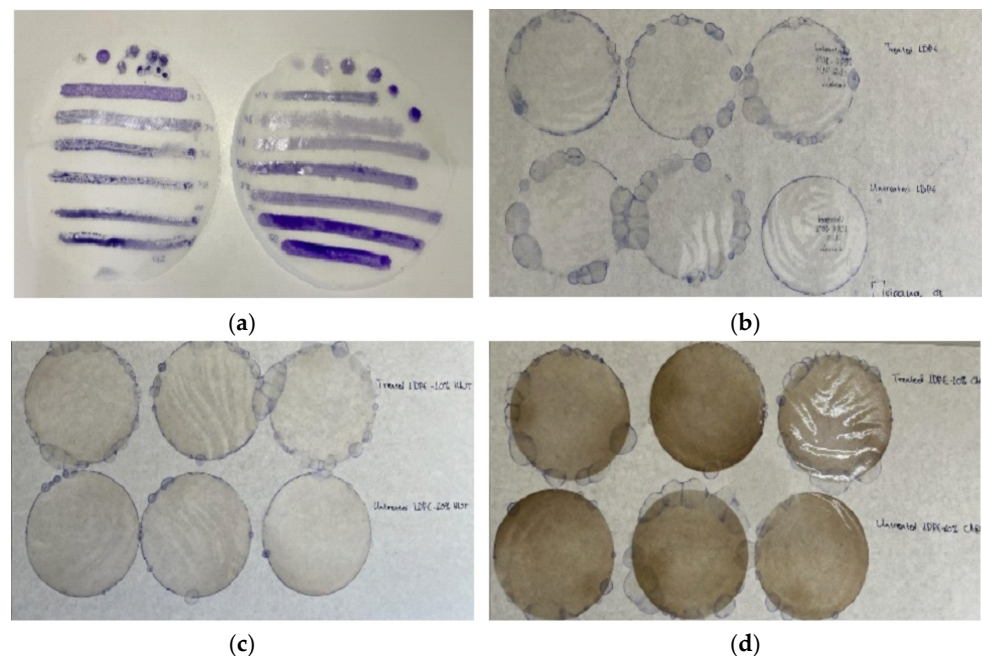


Figure 1. (a) LDPE disk-shaped (11 cm diameter) films tested with special marker pens for wettability measurements before applying the corona treatment; (b) three LDPE films corona treated and coated with CV (upper part), and three LDPE untreated films coated with CV (lower part); (c) three LDPE/10HNT films corona treated and coated with CV (upper part), and three LDPE/10HNT untreated films coated with CV (lower part); and (d) three LDPE/10CV@HNT films corona treated and coated with CV (upper part), and three LDPE/10CV@HNT untreated films coated with CV (lower part).

2.4. Preparation of CV Surface-Coated Films

The obtained “blank” LDPE, LDPE/HNT, and LDPE/CV@HNT films were surface coated with CV with two different treatments. One batch of LDPE, LDPE/HNT, and LDPE/CV@HNT films were surface coated with CV by spreading CV on the external side of the films with a paintbrush. This batch of films is denoted as untreated CV-coated films (see Table 1). A second batch of LDPE, LDPE/HNT, and LDPE/CV@HNT films were firstly corona treated for 30 s by employing a Handheld Corona Surface Treater Model BD-20 V supplied by Electronic-Technic Products (4642 North Ravenswood Ave. Chicago, IL 60640-4510, USA). The 30 s corona treatment time was chosen as the optimum time after the wettability tests carried out in all LDPE, LDPE/HNT, and LDPE/CV@HNT films by using the special wettability marker pens supplied by Diversified Enterprises, Claremont, NH, USA (see Figure 1a). Its special wettability marker corresponds to one wettability value in din/cm. So, the 30 s of the corona treatment process was the optimum treatment time to reach the value of 50–52 din/cm wettability which is reported to be the proper wettability value to turn a hydrophobic LDPE surface hydrophilic (see Figure 1a) [43,44,52]. The obtained films after the corona treatment and surface coating with CV were labeled as corona-treated CV-coated films (see Table 1). For each untreated and corona-treated CV-coated film with an 11 cm diameter (see Figure 1), 500 μ L of CV was used for the coating process and the coating was performed by using a paintbrush.

Table 1. Code names of all films developed in the current study, amounts of LDPE, HNT, CV@HNT, and CV used, and twin extrusion and corona treatment applied conditions.

	LDPE(g)	HNT(g)	CV@HNT(g)	Twin Extrusion Process Time (min)-Speed (rpm)	Corona Treatment Process Time (s)	CV (μ L)
LDPE	4.5	-	-	3-100	-	-
LDPE/10HNT	4.5	0.5	-	3-100	-	-
LDPE/10CV@HNT	4.5	-	0.5	3-100	-	-
un-LDPE_CV	4.5	-	-	3-100	-	500
un-LDPE/10HNT_CV	4.5	0.5	-	3-100	-	500
un-LDPE/10CV@HNT_CV	4.5	-	0.5	3-100	-	500
tr-LDPE_CV	4.5	-	-	3-100	30	500
tr-LDPE/10HNT_CV	4.5	0.5	-	3-100	30	500
tr-LDPE/10CV@HNT_CV	4.5	-	0.5	3-100	30	500

2.5. Fourier Transform Infrared (FTIR) Measurements

All the obtained films as well as pure CV, pure HNT, and modified CV@HNT nanohybrid were characterized with FTIR spectroscopy by employing an FT/IR-6000 JASCO Fourier transform spectrometer (JASCO, Interlab, S.A., Athens, Greece). Typical experimental conditions are set as follows: wavenumber range from 4000 to 400 cm^{-1} and the obtained spectrum was the average of 45 scans at 1 cm^{-1} resolution.

FTIR spectroscopy was used to investigate possible changes in the chemical composition of corona-treated films. For this reason, a batch of the obtained “blank” LDPE, LDPE/HNT, and LDPE/CV@HNT films were surface corona treated for 30 s and immediately measured with FTIR spectroscopy. The obtained FTIR plots are compared with the FTIR plots of the LDPE, LDPE/HNT, and LDPE/CV@HNT films before the surface treatment.

FTIR spectroscopy was used as a key method to investigate the possible interaction between CV-coated molecules and chemical groups of all obtained treated and untreated films. For this reason, FTIR plots of un-LDPE_CV, un-LDPE/10HNT_CV, and un-LDPE/10CV@HNT_CV films were compared with the FTIR plots of tr-LDPE_CV, tr-LDPE/10HNT_CV, and tr-LDPE/10CV@HNT_CV films.

FTIR spectroscopy was used to study the release process of CV from the surface of all obtained films. For such experiments, a sample of each untreated film coated with

CV (un-LDPE_CV, un-LDPE/10HNT_CV, un-LDPE/10CV@HNT_CV) and a sample of each film treated with corona and coated with CV (tr-LDPE_CV, tr-LDPE/10HNT_CV, and tr-LDPE/10CV@HNT_CV) was kept under ambient conditions and measured for its FTIR spectrum every day for 2 weeks total time.

2.6. Tensile Properties of Films

To investigate the mechanical properties of all the obtained films, tensile measurements were carried out according to the ASTM D638 method and the methodology described in detail recently by using a Simantzü AX-G 5kNt instrument (Simantzü. Asteriadis, S.A., Athens, Greece) [47].

2.7. Water/Oxygen Barrier Properties of Obtained Films

2.7.1. Water Vapor Transmission Rate (WVTR) and Water Vapor Diffusion Coefficient (D_{wv})

The WVTR ($\text{g}/\text{cm}^2 \cdot \text{s}$) for all obtained films was measured according to the ASTM E96/E 96M-05 method at 38°C and 95 of %RH by using a handmade apparatus. The calculated WVTR values were transformed to D_{wv} values according to the theory described in detail recently by using the following Equations (1) and (2) [46,53]:

$$\text{WVTR} = \Delta G/t \cdot A \quad (1)$$

where ΔG (g) is the increase in weight of the tested tubes, t (s) is the time pass, $\Delta G/t$ (g/s) is the water transmission rate through the film which is calculated with the slope of the linear function $\Delta G = f(t)$, and A (cm^2) is the permeation area of the film.

$$D_{wv} = \text{WVTR} \cdot (\Delta x / \Delta C) \quad (2)$$

where WVTR [$\text{g}/(\text{cm}^2 \cdot \text{s})$] is the water vapor transmission rate, Δx (cm) is the film thickness, and ΔC (g/cm^3) is the humidity concentration gradient in the two opposite sides of the film.

2.7.2. Oxygen Transmission Rate Measurements and Oxygen Permeability

Oxygen Transmission Rate (OTR) values ($\text{cc O}_2/\text{m}^2/\text{day}$) for all obtained films were measured according to the ASTM D 3985 method at 23°C and 0% of RH by employing an oxygen permeation analyzer (O.P.A., 8001, Systech Illinois Instruments Co., Johnsburg, IL, USA). From the measured OTR values, the oxygen permeability coefficient values (P_{eO_2}) were calculated according to the theory provided in detail recently and Equation (3) [46,53]:

$$P_{eO_2} = \text{OTR} \cdot \Delta x \quad (3)$$

where Δx is the average film thickness.

2.8. Control Release Kinetics Studies of CV from Obtained Films

For all obtained films, the release rate of CV was determined by using a moisture analyzer AXIS AS-60 (AXIS Sp. z o.o. ul. Kartuska 375b, 80-125 Gdańsk, Poland) according to the methodology described previously [42]. Approximately 500 to 700 mg of each film was used for each control release experiment. For each film, at least three samples were measured. Each film was placed inside the moisture analyzer, and its mass was monitored by heating at 70°C for 1 h. With the obtained film mass values (m_t) as a function of time (t) the $\mu\text{g}/\text{s}$ CV release rate (R_{cv}) as well as the %wt. CV, released content (% RC_{cv}) was determined for each film. R_{cv} and % RC_{cv} were determined by using the following Equations (4) and (5):

$$R_{cv} = (m_i - m_f)/t_{\text{total}} \quad (4)$$

$$\%RC_{cv} = (m_i - m_f)/m_i \times 100 \quad (5)$$

where m_i is the initial mass of film, m_f is the final mass of film, and t_{total} is equal to 3600 s.

2.9. Antioxidant Activity of Films

For all antioxidant activity experiments, a standard solution of 2,2-diphenyl-1-picrylhydrazyl radical [DPPH•] was prepared by devolving 0.0212 g of [DPPH•] free radical in 250 mL of methanol to obtain a 2.16 mM (mmol/L) [DPPH•] free radical methanolic solution. Next, the flask was closed tightly and stirred under dark condition for 12 h to ensure the complete dissolution of [DPPH•] free radical, and its pH was measured to ensure its neutrality (7.02 ± 0.01).

Next a calibration curve of [DPPH•] free radical was made by diluting the 2.16 mM (mmol/L) methanolic solution of [DPPH•] free radical to obtain methanolic solutions with concentrations up to 5, 10, 20, 30, and 40 mg/L. Then, the absorbance of the obtained diluted methanolic solution of [DPPH•] free radical was measured at 517 nm by employing a SHIMADZU UV-1280 UV/VIS Spectrometer. The calibration curve of absorbance (y) versus concentration (x) of [DPPH•] free radical was expressed with the following Equation (6):

$$y = 0.0388x + 0.015; R^2 = 0.9994 \quad (6)$$

2.9.1. Total Antioxidant Activity of Films

The antioxidant activity of all obtained LDPE/xTEO@SBA-15 active films was measured using the 2,2-diphenyl-1-picrylhydrazyl radical (DPPH) assay, as described previously [48,54,55]. Briefly, in 2.8 mL of 30 ppm DPPH ethanolic solution, 0.2 mL of $\text{CH}_3\text{COONa} \cdot 3\text{H}_2\text{O}$ of buffer solution and approximately 2 mg of each LDPE/xTEO@SBA-15 active film was added, and the absorbance at 517 nm was recorded as a function of time every day for 1 week total time. As a blank sample, the absorbance of 4 mL of 30 ppm DPPH methanolic solution without the addition of any film was also recorded as a function of time. The % antioxidant activity was calculated by using Equation (7):

$$\% \text{ DPPH scavenged at steady state} = (A_{0-517} - A_{\text{sample-517}}) / A_{0-517} \times 100 \quad (7)$$

where A_{0-517} is the absorbance at 517 nm of the first sample at time 0 s and $A_{\text{sample-517}}$ is the absorbance of each next sample at 517 nm at time t .

2.9.2. Determination of the Effective Concentration (EC₅₀) of Obtained Films

For the determination of concentration required to obtain 50% antioxidant effect (EC₅₀) of all obtained films, 10, 20, 30, 40, and 50 mg of small pieces of each film were placed in dark vials, and three replicates were performed for each sample. Thereafter, 3 mL of [DPPH•] free radical methanolic solution and 2 mL of acetate buffer 100 mM (pH = 7.10) were added to each vial and the absorbance of the reaction mixture was measured at 517 nm after 24 h. For the preparation of the blank sample, a vial was used where 3 mL of [DPPH•] free radical methanolic solution and 2 mL of acetate buffer was added without the addition of any granule film. The % of inhibition of [DPPH•] was calculated using Equation (7).

2.10. Statistical Analysis

All acquired structural, mechanical, antioxidant, and control release kinetic properties were measured experimentally in triplicate and were subjected to statistical analysis for descriptive statistic values calculations. Furthermore, multiple comparison tests were carried out using the Kruskal–Wallis routine to investigate statistical equalities or differences of mean values. Statistical measurements were conducted with a least significance level of $p < 0.05$ using SPSS software (v. 28.0, IBM, Armonk, NY, USA).

3. Results

3.1. FTIR Characterization

In Figure 2 the FTIR plots of pure CV, pure HNT, and modified CV@HNT nanohybrid are presented for comparison.

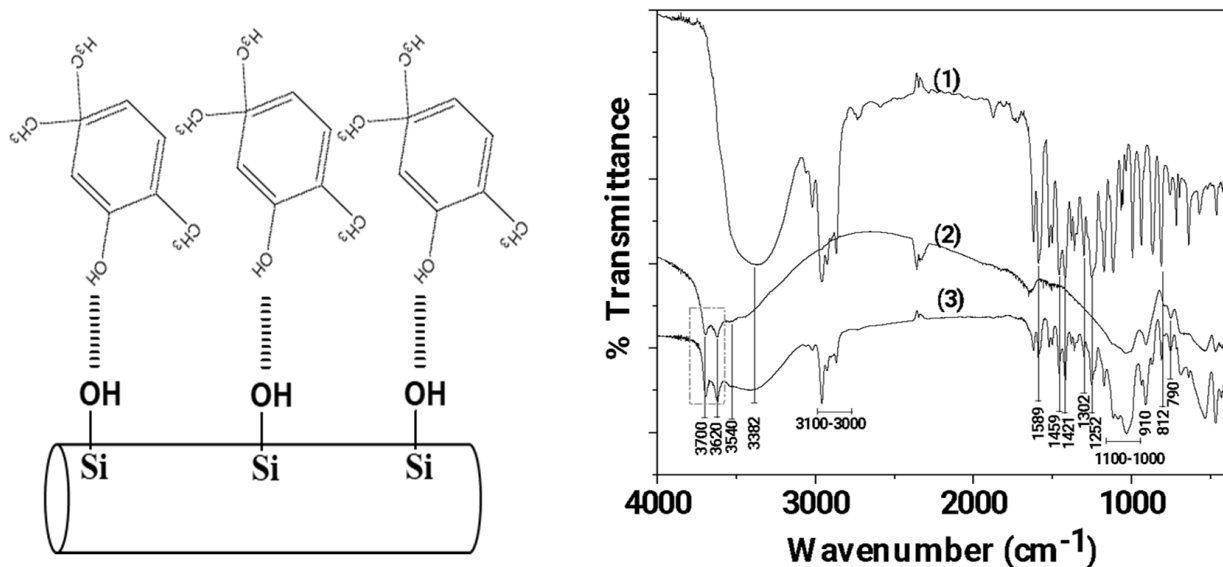


Figure 2. Left part: Schematic illustration of CV molecules adsorbed on HNT, Right part: FTIR plots of (1) pure CV, (2) pure HNT, and modified (3) CV@HNT nanohybrid.

Figure 2 (line 1) illustrates the spectral analysis of pure CV, whereby the presence of the O-H groups is indicated by the broad peak at 3382 cm^{-1} [56,57]. The stretching vibrations of aromatic and alkenic $-\text{CH}=\text{CH}-$ are observed as bands in the region $\sim 3100\text{--}3000\text{ cm}^{-1}$ [56,57]. The band at 1589.83 cm^{-1} is assigned to the stretching vibration of a C-C bond; the bands at 1459 and 1421 cm^{-1} are assigned to the bending vibration of OH groups; the band at 1302 cm^{-1} is assigned to the isopropyl group $\text{C}(\text{CH}_3)_2$; the band at 1252 cm^{-1} is assigned to the stretching vibration of a C-O-C group; and the band at 812 cm^{-1} is assigned to the bending vibration of an aromatic C-H bond [56,57].

In the FTIR plot of pure HNT (see the line 2 in Figure 2), the bands at 3700 and 3620 cm^{-1} are assigned to the stretching vibration of hydroxyl groups located in the internal surface of HNT [58,59]. The Si-O-Si (Al) groups appear as a weak band at 3540 cm^{-1} [58], while the Si-O groups appear as intense bands from 1100 to 1000 cm^{-1} and at 790 cm^{-1} [59]. The band at 910 cm^{-1} is assigned to the bending vibration of the inner hydroxyl group [59]. Finally, the band at 745 cm^{-1} is assigned to the Si-O-Al bonds [58,59].

The FTIR plot of the CV@HNT nanohybrid is a mix of both of pure CV and pure HNT plots. With a careful glance, it is observed that the bands at 3700 and 3620 cm^{-1} , which are attributed to internal surface located hydroxyl groups of HNT, are increased in the FTIR plot of CV@HNT as compared to the FTIR plot of pure HNT. This reveals an interplay between the hydroxyl groups of CV and hydroxyl groups of HNT located in the external surface as it is illustrated in Figure 1.

In Figure 3, the FTIR plots of pure CV as well as LDPE, LDPE/10HNT, and LDPE/10CV@HNT films are shown for comparison.

In the FTIR plot of pure LDPE film (see plot line (2) in Figure 3), the characteristic peaks of LDPE at 2913 , 2844 , 1460 , and 715 cm^{-1} are observed [60]. The peaks at 2913 and 2844 cm^{-1} are assigned to the symmetric stretching vibration of the $-\text{CH}_2$ group of LDPE, while the peaks at 1460 and 715 cm^{-1} are assigned to the wagging and rocking vibration of the $-\text{CH}_2$ group of LDPE, correspondingly [61]. In the FTIR plot of the LDPE/10HNT film (see plot line (3) in Figure 3), the characteristic bands of HNT at 3700 , 3620 , 910 , and in the range of $1100\text{--}1000\text{ cm}^{-1}$ are observed along with the characteristic bands of LDPE. In the FTIR plot of the LDPE/10CV@HNT film (see plot line (4) in Figure 3), the characteristic bands of CV at 3382 , 1589 , 1421 , 1302 , 1252 , 910 , 812 , and 790 cm^{-1} are observed along with the characteristic bands of LDPE and HNT. No LDPE peak shift is observed in both the LDPE/10HNT and LDPE/10CV@HNT films according to previous similar reports [47,62].

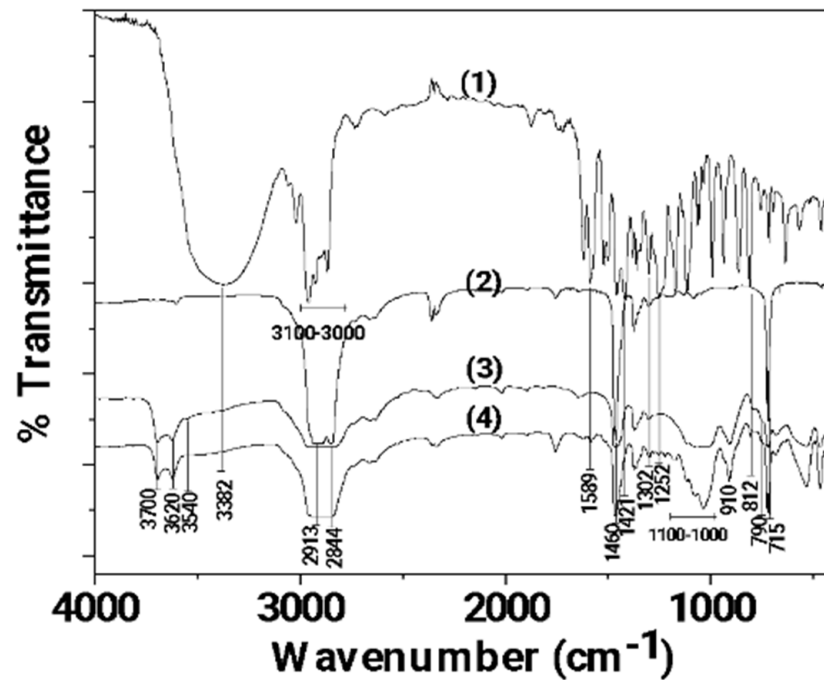


Figure 3. FTIR plots of (1) pure CV as well as (2) LDPE, (3) LDPE/10HNT, and (4) LDPE/10CV@HNT films.

In Figure 4, the FTIR plots of pure LDPE, LDPE/10HNT, and LDPE/10CV@HNT untreated (black lines) and corona-treated (blue lines) films are shown for comparison.

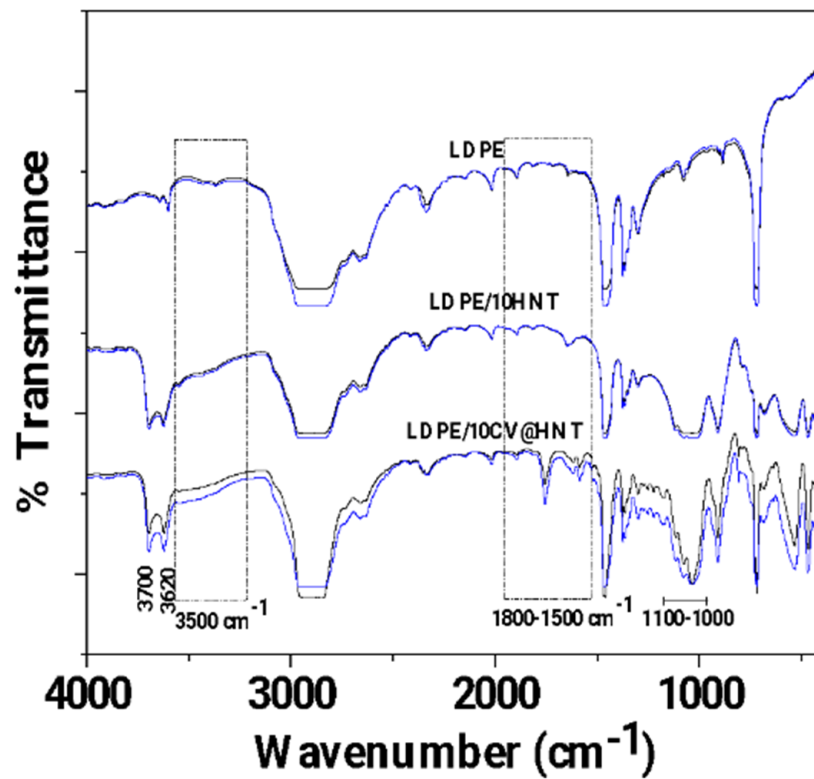


Figure 4. FTIR plots of pure LDPE, LDPE/10HNT, and LDPE/10CV@HNT untreated (black lines) and corona treated (blue lines).

With a first glance, it is observed that in all cases, FTIR plots of all corona-treated samples (blue lines) are increased as compared to FTIR plots of all untreated samples (black

lines). This is direct evidence of the surface activation achieved with corona treatment in the case of all tested films. According to the literature, the increase in bands at 3500 cm^{-1} (see dash dot rectangle region in Figure 4) is evidence of incorporated oxygen-containing functional groups (-OH). The increase in bands in the range $1800\text{--}1500\text{ cm}^{-1}$ (see dash dot rectangle region in Figure 4) is evidence of oxygen species incorporated in a carbonylic group (-C=O), while the increase in the absorbance band with a maximum at 1730 cm^{-1} is evidence that carboxylic acids appeared [59]. With a more careful glance, it is observed that there is a higher activation in the case of both LDPE/10HNT and LDPE/10CV@HNT samples as compared to pure LDPE film. Additional activated sites are observed in the case of both LDPE/10HNT and LDPE/10CV@HNT corona-treated samples. These are the bands at 3700 and 3620 , and the bands in the range of 1100 to 1000 cm^{-1} corresponded to surface and inner hydroxyl groups of HNT. In the case of the LDPE/10CV@HNT corona-treated sample, extra active sites are observed in the range of 2000 to 400 cm^{-1} , corresponding to CV. Thus, it seems that in the case of LDPE/10HNT and LDPE/10CV@HNT corona-treated samples, additional oxygen species are incorporated in the hydroxyl groups of HNT for both LDPE/10HNT and LDPE/10CV@HNT samples and in the hydroxyl groups of both HNT and CV molecule for the LDPE/10CV@HNT sample. In other words, the incorporation of both the HNT and CV@HNT nanohybrid in the LDPE matrix leads to a final matrix with more active sites available for incorporation of oxygen species via the corona treatment process.

In Figure 5, the FTIR plots of pure LDPE, un-LDPE_CV, and tr-LDPE_CV films are presented for comparison.

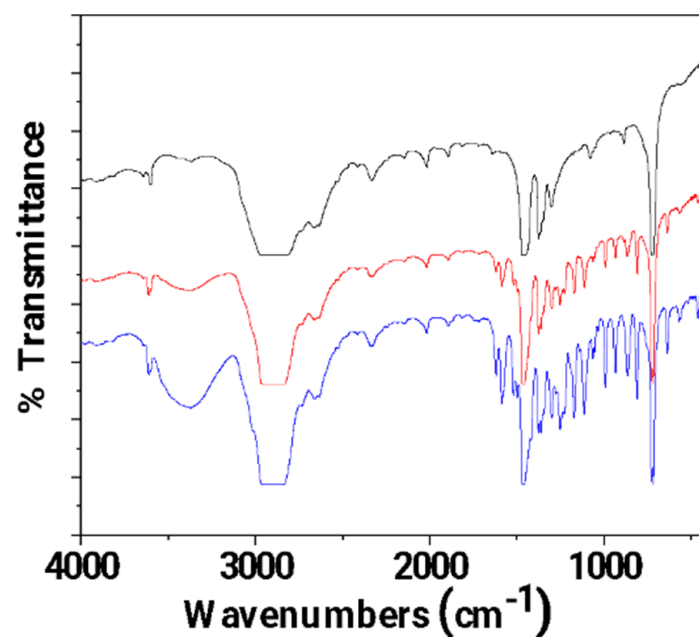


Figure 5. FTIR plots of pure LDPE (black line), un-LDPE_CV (red line), and tr-LDPE_CV (blue line) films.

It is obvious that in the FTIR plot of the tr-LDPE_CV film, the bands corresponding to CV molecules (see the broad band at 3500 cm^{-1} and the bands in the range of $2000\text{--}400\text{ cm}^{-1}$) are higher as compared to the FTIR plot of the un-LDPE_CV film. This is direct proof that corona treatment activates the LDPE surface and results in a higher amount of adsorbed CV in the case of the tr-LDPE_CV film as compared to the amount of CV adsorbed in the case of the un-LDPE_CV film.

In Figure 6, the FTIR plots of pure LDPE/10HNT, un-LDPE/10HNT_CV, and tr-LDPE/10HNT_CV films are presented for comparison.

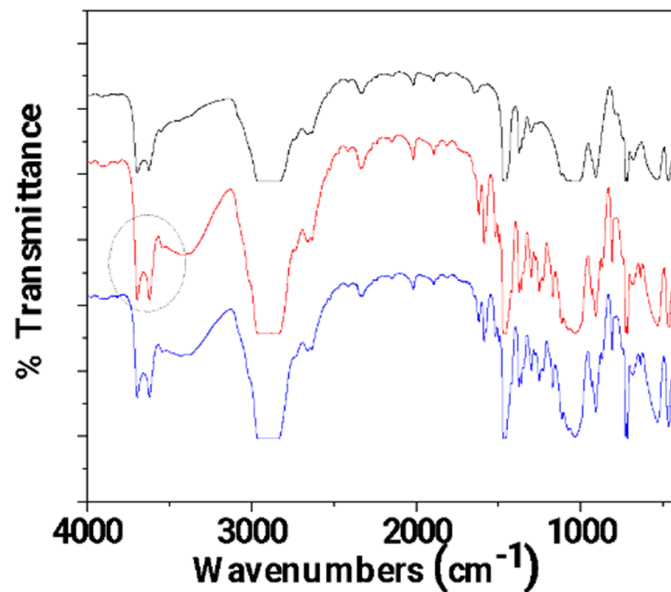


Figure 6. FTIR plots of pure LDPE/10HNT (black line), un-LDPE/10HNT_CV (red line), and tr-LDPE/10HNT_CV (blue line) films.

In Figure 6, it is observed that the bands corresponding to CV molecules (see the broad band at 3500 cm^{-1} and the bands in the range of $2000\text{--}400\text{ cm}^{-1}$) are almost equal for both un-LDPE/10HNT_CV and tr-LDPE/10HNT_CV. This means that both corona-treated and untreated LDPE/10HNT films adsorbed almost equal amounts of CV. This result seems controversial at first as it could be expected that corona treatment should lead to the adsorption of higher amounts of CV in the case of tr-LDPE/10HNT_CV as compared to the adsorbed amount of CV in the case of the un-LDPE/10HNT_CV film. With a more careful glance at the FTIR plot of un-LDPE/10HNT_CV, it is observed that the bands at 3700 and 3620 cm^{-1} (see the region denoted with the gray colored dash dot circle) corresponding to the hydroxyl groups of HNT located in the external surface are much higher as compared to the same bands in the case of the FTIR plot of the pure LDPE/10HNT film. This activation of HNT's hydroxyl groups suggests a relaxation of the hydroxyl groups with the coated molecules of CV. Thus, it seems that the presence of HNT in the LDPE/10HNT film increases the active sites where CV molecules can be adsorbed, and thus, the obtained un-LDPE/10HNT_CV film with coated CV molecules adsorbed equal amounts of CV molecules as compared to the amount of CV molecules adsorbed in the case of the corona-treated tr-LDPE/10HNT_CV film.

In Figure 7, the FTIR plots of pure LDPE/10CV@HNT, un-LDPE/10CV@HNT_CV, and tr-LDPE/10CV@HNT_CV films are presented for comparison.

In Figure 7, it is observed that the bands corresponding to CV molecules (see the broad band at 3500 cm^{-1} and the bands in the range of $2000\text{--}400\text{ cm}^{-1}$) are almost equal for both un-LDPE/10CV@HNT_CV and tr-LDPE/10CV@HNT_CV as in the case of un-LDPE/10HNT_CV and tr-LDPE/10HNT_CV films. Also, the same activation in the bands of HNT's external surface-located hydroxyl groups (see the bands at 3700 and 3620 cm^{-1} denoted with the gray colored dash dot circle) in the FTIR plot of the un-LDPE/10CV@HNT_CV film, as in the case of the un-LDPE/10HNT_CV film, is observed. Thus, it seems that the presence of the CV@HNT nanohybrid in the LDPE/10CV@HNT film increases the active sites where CV molecules can be adsorbed because of the presence of CV molecules inside the LDPE/10CV@HNT film and because of the presence of hydroxyl groups sited in the external surface of HNT. As a result, the obtained un-LDPE/10CV@HNT_CV film with coated CV molecules adsorbed equal amounts of CV molecules as compared to the corona-treated tr-LDPE/10CV@HNT_CV film.

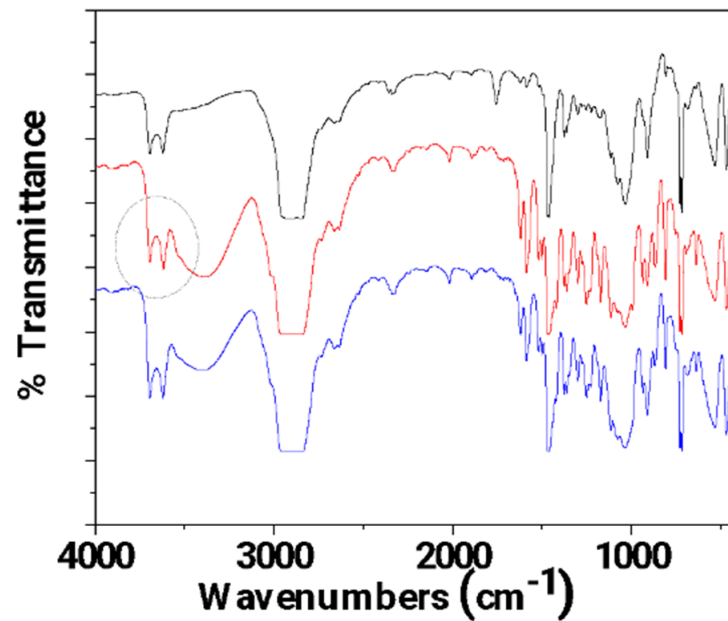


Figure 7. FTIR plots of pure LDPE/10CV@HNT (black line), un-LDPE/10CV@HNT_CV (red line), and tr-LDPE/10CV@HNT_CV (blue line) films.

In Figure S1, the FTIR plots of untreated and coated-with-CV films (un-LDPE_CV, un-LDPE/10HNT_CV, un-LDPE/10CV@HNT_CV) and corona-treated and coated-with-CV films (tr-LDPE_CV, tr-LDPE/10HNT_CV and tr-LDPE/10CV@HNT_CV) on day 1, day 2, day 3, day 4, day 7, day 9, day 11, and day 14 are shown for comparison. For better comparison, the same FTIR plots have been zoomed in the range of 1440 to 400 cm^{-1} where the most bands of CV molecules are observed as shown in Figure 8.

Comparing the FTIR plots of the un-LDPE_CV film (see graph (a) in Figure 8) and tr-LDPE_CV (see graph (b) in Figure 8), it is obvious that, in the case of the un-LDPE_CV film, the CV molecules released quickly and are not detected in the surface of the un-LDPE_CV film after the fourth day (see the region marked with rectangle with dotted lines). On the contrary, in the case of tr-LDPE_CV, the release of CV molecules is slower, and the CV molecules are detectable on the surface of tr-LDPE_CV up to the 11th day. In the case of the un-LDPE/10HNT_CV (see graph (c) in Figure 8), tr-LDPE/10HNT_CV (see graph (d) in Figure 8), un-LDPE/10CV@HNT_CV (see graph (e) in Figure 8), and tr-LDPE/10CV@HNT_CV (see graph (f) in Figure 8) films, the release of CV molecules is slower and the bands of CV molecules are detectable on the surface of un-LDPE/10HNT_CV, tr-LDPE/10HNT_CV, un-LDPE/10CV@HNT_CV, and tr-LDPE/10CV@HNT_CV films up to the 14th day (see the denoted with gray dash dot line rectangle band of CV at 812 cm^{-1}). This result is in accordance with the discussion mentioned hereabove where it was suggested that the presence of active sites of HNT in the un-LDPE/10HNT_CV film and the presence of active site of both HNT and CV molecules in the un-LDPE/10CV@HNT_CV film makes such films able to adsorb equal amounts of CV as the tr-LDPE/10HNT_CV and tr-LDPE/10CV@HNT_CV films, correspondingly. Results presented here by using FTIR analysis as a key method for the determination of CV release from all obtained active films are inspired by a similar report where the concentration of the active compounds of the EOs, i.e., carvacrol, thymol, and p-cymene, was directly calculated in essential oils of oregano and thyme as well as in the antimicrobial LDPE films in which the studied EOs were incorporated using a simple FTIR analysis method [57].

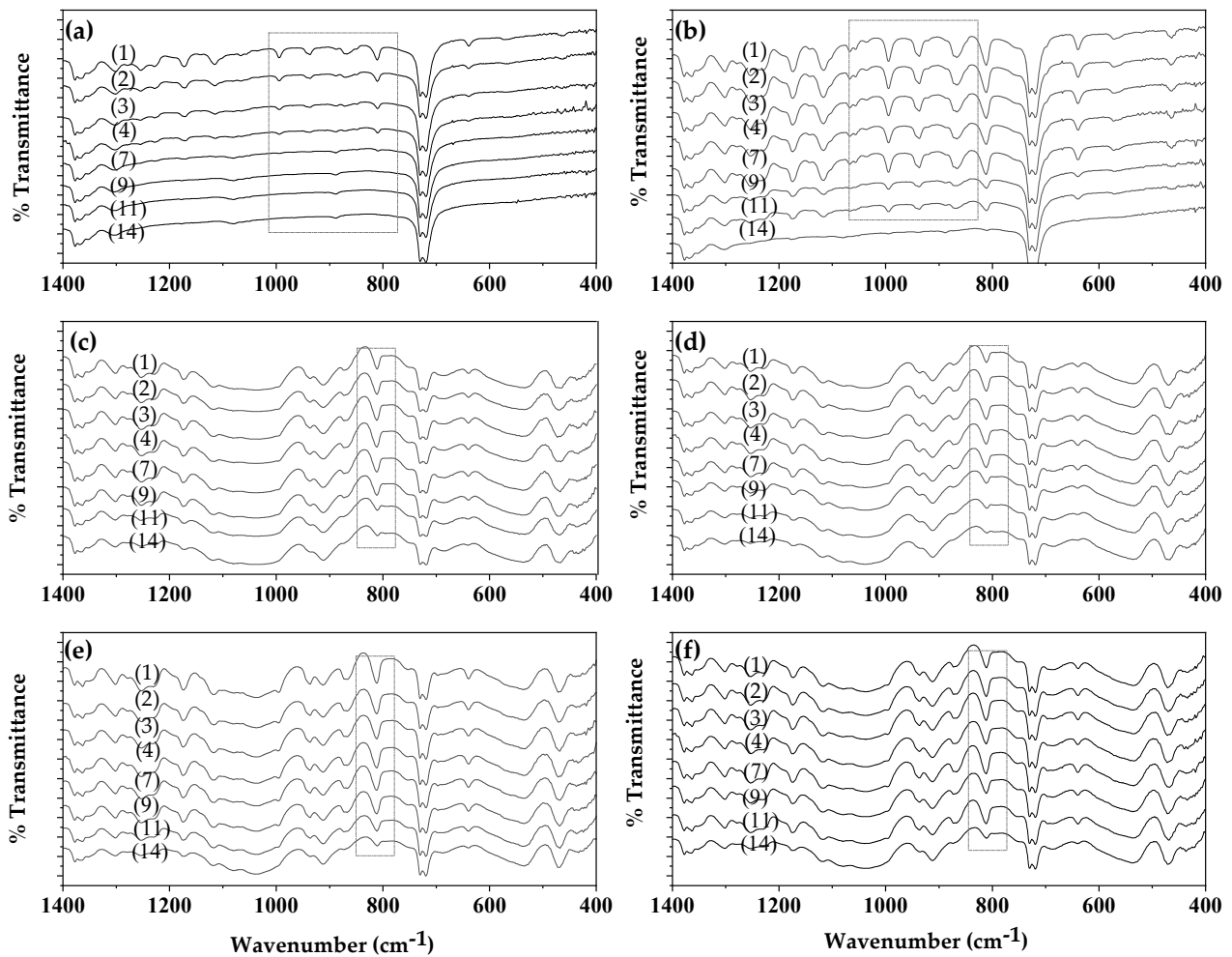


Figure 8. FTIR plots of (left column of graphs): untreated and coated-with-CV films, (a) un-LDPE_CV, (c) un-LDPE/10HNT_CV, (e) un-LDPE/10CV@HNT_CV, and of (right column of graphs) corona-treated and coated-with-CV films, (b) tr-LDPE_CV, (d) tr-LDPE/10HNT_CV, and (f) tr-LDPE/10CV@HNT_CV, on day 1, day 2, day 3, day 4, day 7, day 9, day 11, and day 14.

3.2. Tensile Properties

Table S1 includes the calculated values of the Young's Modulus (E), ultimate strength (σ_{uts}), and elongation at break ϵ (%) for all tested films. For comparison, the same values were plotted in column bar diagrams in Figure 9.

As it is obtained from the calculated Young's Modulus (E), ultimate strength (σ_{uts}), and % elongation at break values in Table S1 and Figure 9, the addition of pure HNT and CV@HNT nanohybrid enhances both stress and ultimate strength and decreases ductility of the obtained LDPE/10HNT and LDPE/10CV@HNT films, implying the creation of a nanocomposite nanostructure in accordance with previous reports [47]. On the other hand, when the surface CV nanocoating is applied, stress and strength values are decreased both in CV-coated-treated and untreated samples as compared to uncoated samples. For un-LDPE_CV and tr-LDPE_CV samples, ductility does not significantly change as compared to pure LDPE film, while for un-LDPE/10HNT_CV, un-LDPE/10CV@HNT_CV, tr-LDPE/10HNT_CV, and tr-LDPE/10CV@HNT_CV films, ductility is significantly decreased as compared to the ductility of LDPE/10HNT and LDPE/10CV@HNT films.

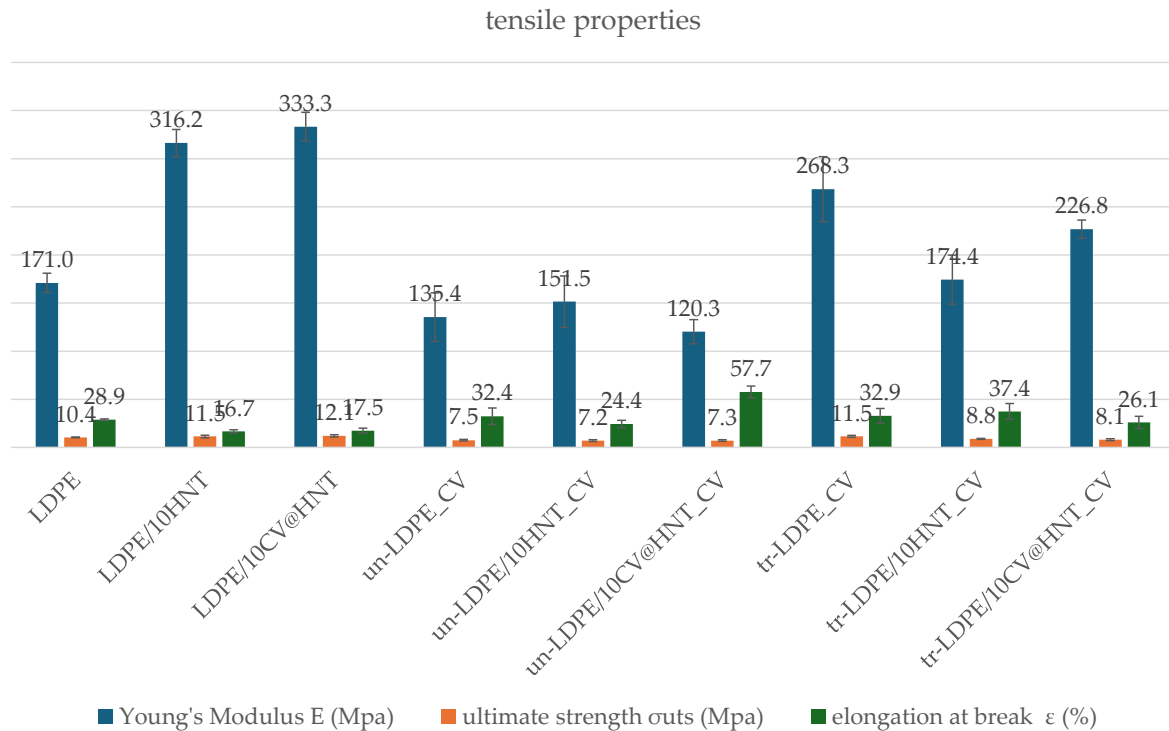


Figure 9. Tensile properties column bar diagrams of (blue column) Young's Modulus, E; (green column) ultimate strength, σ_{uts} ; and (red column) elongation at break values of all tested films.

3.3. Water/Oxygen Barrier Properties

Supplementary Table S2 presents summarizing comparisons between water vapor transmission rate (WVTR) and oxygen transmission rate (OTR) mean values of all tested films. Water vapor diffusion coefficient (D_{wv}) values and the oxygen permeability coefficient (P_{eO_2}) values were calculated from the above corresponding rates and are also listed in Table S2. For ease of comparison, the obtained D_{wv} and P_{eO_2} values are also plotted in the column bar diagram in Figure 10.

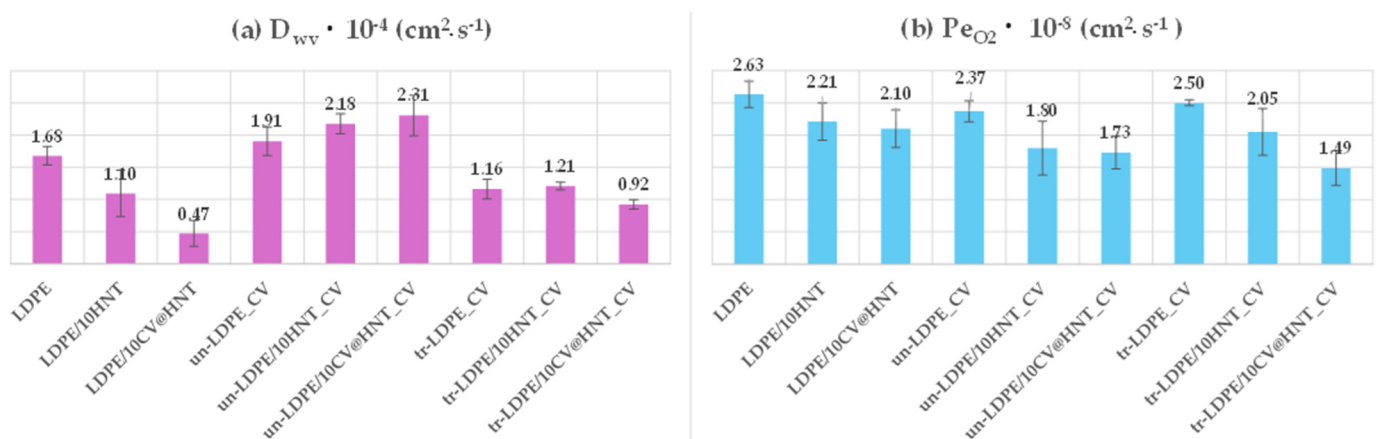


Figure 10. Column bar diagrams of obtained (a) D_{wv} and (b) P_{eO_2} values for all tested films.

From the water vapor diffusion coefficient (D_{wv}) values plotted in Figure 10a, it is obtained that addition of both pure HNT and CV@HNT nanohybrid increases the water barrier of obtained LDPE/10HNT and LDP/10CV@HNT nanocomposite films. This result is well known when a nanoclay such as HNT or a hybrid such as CV@HNT are incorporated in polymer films [47,63,64]. But the aim of this study was to incorporate the CV natural preservative in the commercially used LDPE matrix and avoid causing significant defects

in other mechanical and physicochemical properties. Thus, in this study, we focused mainly on the barrier differences between treated and untreated CV-coated films. The film surface nanocoating with CV, using or not using corona treatment, seems to have controversial results in the water barrier properties. The un-LDPE_CV film exhibited no significant difference in water barrier values as compared to the pure LDPE film. The un-LDPE/10HNT_CV and the un-LDPE10/CV@HNT_CV films exhibited lower water barrier properties as compared to the pure LDPE film and much lower water barrier as compared to the LDPE/10HNT and LDPE/10CV@HNT films, correspondingly. The tr-LDPE_CV, tr-LDPE/10HNT_CV, and tr-LDPE/10CV@HNT_CV films exhibited higher water barrier properties compared to the values of the pure LDPE film which, on the other hand, were slightly but not significantly lower compared to the water barrier values of the LDPE/10HNT and LDPE/10CV@HNT films. In addition, all corona-treated films exhibited higher water barrier properties than untreated CV-coated films. This result indicates that the corona treatment process for applying CV nanocoating on the surface of pure LDPE, LDPE/10HNT, and LDPE/10CV@HNT nanocomposite films is appropriate. In general, CV, a compound found in essential oils such as oregano oil, does not have a significant impact on the LDPE polymeric matrix. LDPE is relatively resistant to many chemicals and solvents, including those found in essential oils. However, prolonged exposure or high concentrations of carvacrol could potentially cause some swelling or softening of LDPE over time, but it is unlikely to cause immediate or significant dilution. This could be an explanation for how the CV coating causes a slight decrease in the water and oxygen barrier. According to the experimental results, the corona-treatment procedure offers a kind of protection or deceleration against this phenomenon. A possible explanation for the superiority of corona-treated films compared to the untreated films could be the surface bonding of CV molecules on the corona-treated surface of LDPE, LDPE/10HNT, and LDPE/10CV@HNT nanocomposite films. On the contrary, the naughty or less-bonded CV molecules on the untreated surface of such materials cannot offer similar advantageous behavior.

From the P_{eO_2} values plotted in Figure 10b, it is observed that both corona-treated and untreated films do not exhibit significantly different values as compared to pure LDPE, LDPE/10HNT, and LDPE/10CV@HNT nanocomposite films. Only the film tr-LDPE/10CV@HNT_CV exhibited lower P_{eO_2} values as compared to all the other tested nanocomposite films.

3.4. CV Release Kinetics

The CV release rate (R_{CV}) as well as the wt.% of CV release content ($\%RC_{CV}$) was calculated for all films and listed in Table S3. The recorded values are also plotted in Figure 11 for comparison.

As it is obtained from the values listed in Table S3, all corona-treated samples release lower %wt. CV contents with lower release rates as compared to untreated samples. This result, combined with the FTIR characterization results discussed hereabove, is direct proof that corona treatment leads to a CV surface coating bonded onto the surface of the film, and it is released with a different pace. In addition, from the $\%RC_{CV}$ values listed in Table S3, it is evident that the incorporation of the HNT nanostructure and CV@HNT nanohybrid in the LDPE matrix increased the surface bonding of CV molecules in both corona-treated and untreated active films. This result also is in accordance with the FTIR characterization discussion hereabove (see Figures 6 and 7), where it was shown that the incorporation of both HNT and CV@HNT nanohybrid in the LDPE matrix leads to a final matrix with more active sites available for incorporation of oxygen species via the corona treatment process. A probable explanation of this could be that both HNT and CV@HNT have much more hydroxyl groups in their structure which probably activate much more oxygen species with corona treatment, and such species are available as adsorption active sites. The results of release kinetics presented here are novel for such CV-nanocoated with-or-without-corona-treatment LDPE films but they are comparable with similar results for eugenol release

kinetics studies with chitosan–alginate polyelectrolyte complex and linear low-density polyethylene (LLDPE) film [65,66].

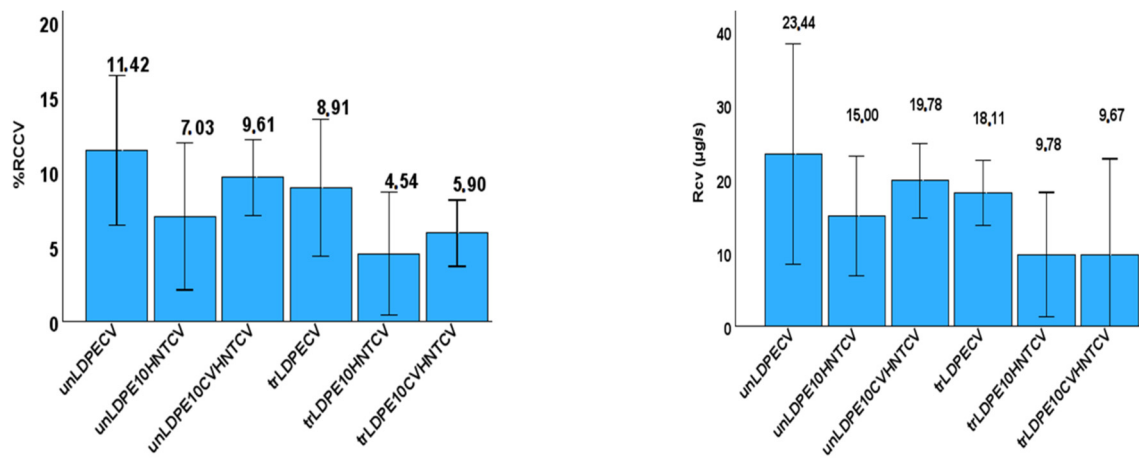


Figure 11. Left part: Column bar diagram with the calculated CV release rate (R_{CV}) values for all tested films; right part: Column bar diagram with the calculated %wt. CV release content (% R_{CCV}) values for all tested films.

3.5. Antioxidant Activity of Films

The calculated total antioxidant activity values of all obtained active films as a function of day are plotted in Figure 12a. The calculated EC_{50} mean values for all obtained active films are plotted in the column bar diagram in Figure 12b and are listed in Table S4.

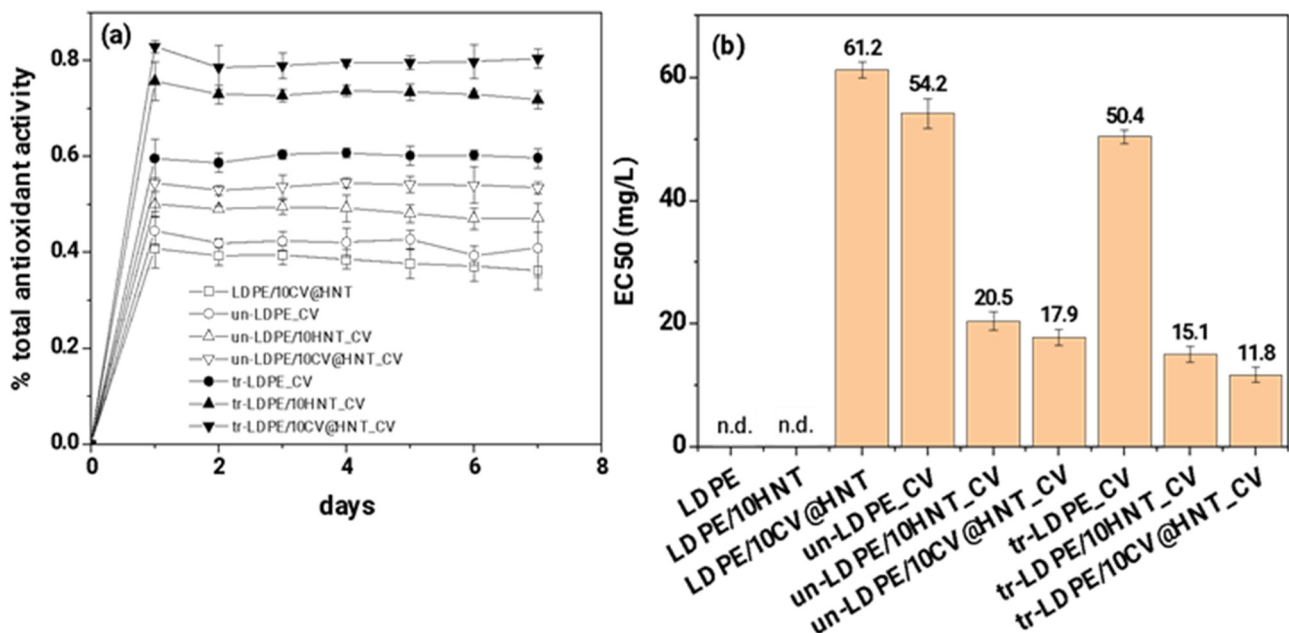


Figure 12. (a) total antioxidant activity of all tested active films as a function of time (days) and (b) mean EC_{50} values for all tested active films (n.d. means no-data).

As it is obtained in Figure 12a,b, both corona-treated and untreated CV-coated samples obtain higher % total antioxidant activity values and lower EC_{50} values than the LDPE/10CV@HNT active film. In addition, all corona-treated CV-coated samples exhibited higher % total antioxidant activity values and lower EC_{50} values than untreated CV-coated samples. This result follows the results of CV release kinetics. It is shown that corona-treated films bond higher amounts of CV which do not release or release at a lower rate

and result in higher antioxidant activity values than untreated CV-coated samples where lower amounts of CV molecules are bonded onto the surface of the film.

4. Discussion

In this work, a pure LDPE film, a LDPE/10HNT nanocomposite film, and an LDPE/10CV@HNT nanocomposite active film were firstly prepared via an extrusion molding method and used as reference materials to develop CV nanocoatings on their surface. A batch of LDPE, LDPE/10HNT, and LDPE/10CV@HNT films were coated with CV on their one site surface without corona treatment to obtain un-LDPE_CV, un-LDPE/10HNT_CV, and un-LDPE/10CV@HNT_CV active films, and another batch of LDPE, LDPE/10HNT, and LDPE/10CV@HNT films were firstly surface activated via the corona treatment process and secondly coated with CV on their one site surface to obtain tr-LDPE_CV, tr-LDPE/10HNT_CV, and tr-LDPE/10CV@HNT_CV. In the next Figure 13, all the obtained CV-coated films are illustrated to support the following discussion.

As it was shown with FTIR measurements of the surface of corona-treated LDPE/10HNT and LDPE/10CV@HNT films, the incorporation of both HNT and CV@HNT nanohybrid in the LDPE matrix leads to a final matrix with more active sites available for regeneration of oxygen species via the corona treatment process (see Figure 13d,f). In addition, FTIR measurement showed that CV-nanocoated and corona-treated LDPE film adsorbed higher amounts of CV molecules than the CV-nanocoated untreated LDPE film because of corona treatment activation (see Figure 13b). This result is in accordance with previous reports [43–45,67,68]. On the other hand, CV-nanocoated with-or-without-corona-treatment LDPE/10HNT and LDPE/10CV@HNT active films adsorbed equal CV amounts because of the presence of additional active sites of pure HNT and CV@HNT nanohybrid (see Figure 13c,e). These results are reported for the first time, as it is the first time that such LDPE/10HNT and LDPE/10CV@HNT nanocomposite matrixes are corona treated and nanocoated with an active compound such as CV molecules. These results were confirmed with the results of the FTIR study on the CV molecules released from the surface of all obtained CV-coated (both treated and untreated) active films. As it was shown, CV released faster from the surface of untreated CV-nanocoated LDPE films than from the surface of CV-nanocoated corona-treated LDPE film, while their seems to be the same release rate from the surface of all CV-nanocoated with-or-without-corona-treatment LDPE/10HNT and LDPE/10CV@HNT active films. To study in more detail the CV molecules' release mechanism, CV release kinetics experiments were carried out. CV release kinetic experiments were in accordance with the FTIR characterization results and confirmed the following: (i) all corona-treated samples release lower wt.% CV contents with lower release rates as compared to untreated samples, (ii) the incorporation of the HNT nanostructure and CV@HNT nanohybrid in the LDPE matrix increased the surface bonding of CV molecules in both corona-treated and untreated active films. Such CV release kinetics experiment results suggest that corona treatment leads to a CV surface coating that is bonded onto the surface of the film which is constant and does not release. The results from the CV release kinetics are supported with antioxidant activity results where it was shown that all corona-treated CV-coated films exhibited higher total antioxidant activity and EC50 values than the untreated CV-coated films. Overall, the active tr-LDPE/10HNT_CV and tr-LDPE/10CV@HNT films are the most promising because they exhibit nanocoated CV that is ready to release. The un-LDPE/10HNT_CV and un-LDPE/10CV@HNT films also exhibited a nanocoated CV amount because of CV molecule bonding with extra surface sites created by HNT and CV@HNT nanohybrids, but the nanocoated CV amount in the case of un-LDPE/10HNT_CV and un-LDPE/10CV@HNT films is lower than the nanocoated CV amount in the case of tr-LDPE/10HNT_CV and tr-LDPE/10CV@HNT films. These two tr-LDPE/10HNT_CV and tr-LDPE/10CV@HNT films also exhibited lower water/oxygen barrier properties than pure LDPE film. Both CV-coated corona-treated films and CV-coated untreated films exhibited lower ultimate strength values than reference materials while their ductility does not statistically significantly change. Overall, the tr-LDPE/10CV@HNT

active film seems to be the most promising as it exhibits an internally deposited fraction of CV and surface-nanocoated CV. This tr-LDPE/10CV@HNT active film exhibited more than a 45% higher water barrier, 43% higher oxygen, and 21.1% lower ultimate strength than pure LDPE film. Last but not least, it must be noted that the use of FTIR spectroscopy to study the release of CV for all obtained corona-treated or untreated coated films was inspired by other similar reports where LDPE films were loaded with EOs [57,66]. Also, the release kinetic method developed and presented here for calculating the CV release rate (R_{CV}) values as well as the %wt. CV release content ($\%RC_{CV}$) values of all corona-treated or untreated CV-coated films is similar to that developed and presented recently by Dhoot et al. [66] where FTIR-ATR spectroscopy and HPLC were used to study the release kinetics of eugenol from LLDPE active films. However, the method developed here for CV release kinetics calculations is fast, simple, and cheap, as it is using a moisture analyzer and does not employ more expensive and more complex instrumentation such as HPLC, FTIR-ATR, and/or Thermogravimetric Analysis (TGA) measurements [65,66].

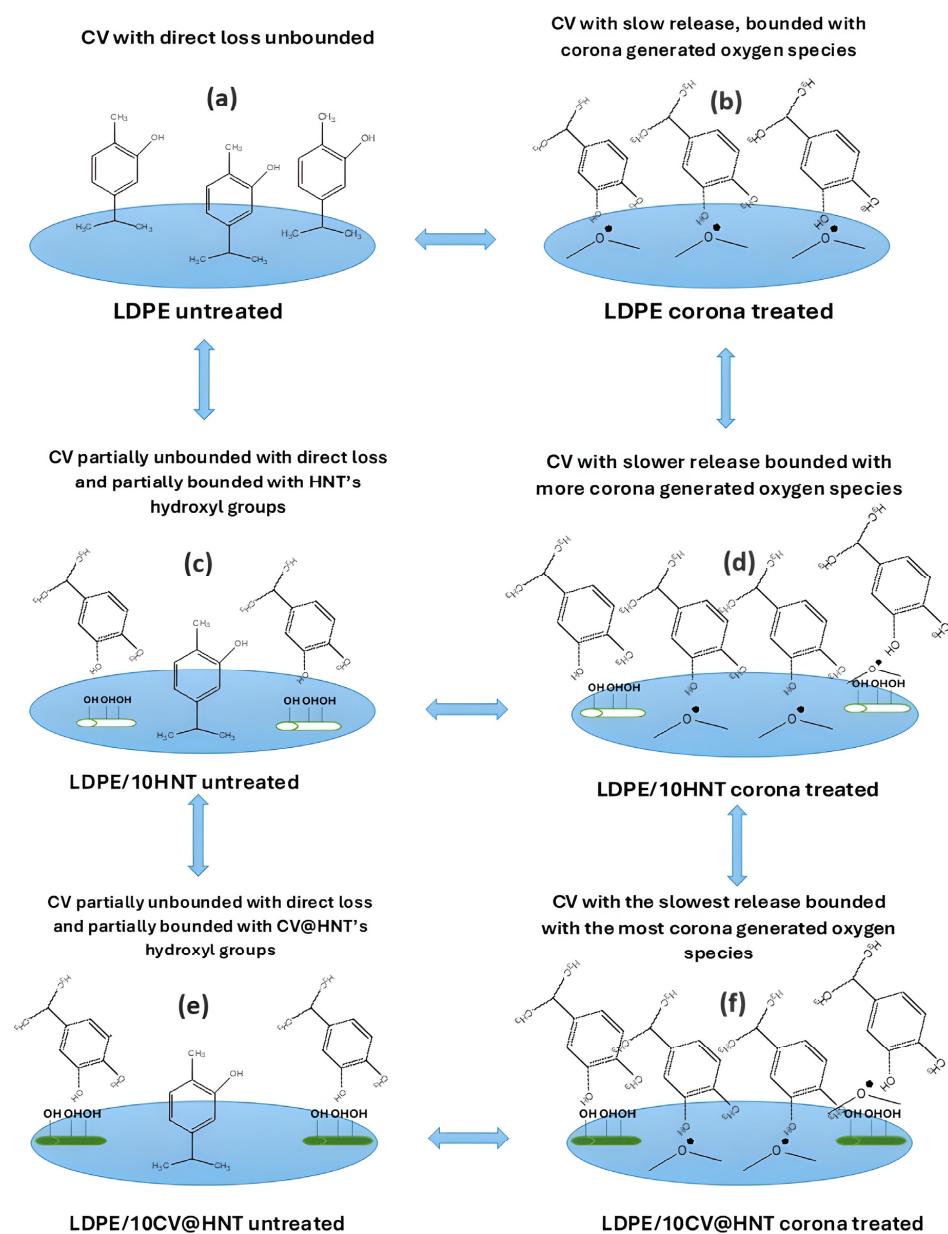


Figure 13. Schematic presentation of all obtained CV nanocoated active films of this study. (a) LDPE untreated, (b) LDPE corona treated, (c) LDPE/10HNT untreated, (d) LDPE/10HNT corona treated, (e) LDPE/10CV@HNT untreated, and (f) LDPE/10CV@HNT corona treated.

5. Conclusions

In this study a novel approach to incorporate essential oils and their derivatives, such as carvacrol, in active food packaging materials is presented. This incorporation is achieved by developing carvacrol nanocoatings on the surface of films of pure low-density polyethylene, incorporated with 10 %wt. halloysite nanotubes, and pure low-density polyethylene incorporated with 10 wt.% halloysite nanotubes impregnated with carvacrol. Extra carvacrol coating was spread on such films surface with and without using the well-known corona treatment technique. All developed materials were characterized instrumentally to determine their physicochemical and packaging properties. The FTIR spectroscopy analyses showed that the incorporation in the low-density polyethylene matrix of halloysite nanotubes, as well as of nanohybrids consisted of halloysite nanotubes impregnated with carvacrol, leads to a final matrix with more active sites available for the regeneration of oxygen species via the corona treatment process. As a result, it was derived that the use of the corona treatment technique led to a higher amount of carvacrol molecules nanocoated on the surface of all tested low-density polyethylene-based films. This happened because of film surface and nanohybrid particle activation via the corona treatment. This result was also verified with carvacrol release kinetic results. According to these results, in all cases of carvacrol nanocoating, with or without corona treatment, a bonded carvacrol nanolayer was created on the films' surface which could not be released. The amount of this bonded carvacrol nanolayer was higher in the case of corona-treated active films. All the obtained carvacrol nanocoated films using the corona treatment technique exhibited higher total antioxidant activity and higher EC50 values compared to carvacrol nanocoated films without using the corona treatment technique. This probably occurs because the carvacrol amount incorporated inside the polymer matrix and another carvacrol amount nanocoated and partially bonded on the external film surface released slowly. The most promising kind of active film seems to be the carvacrol-coated and corona-treated low-density polyethylene film incorporated with 10 %wt. halloysite nanotubes which also were impregnated with carvacrol. This sample exhibited a 45.2% higher water barrier and a 43.3% higher oxygen barrier than the pure LDPE film and could be potentially used as a novel active food packaging film.

Supplementary Materials: The following supporting information can be downloaded at: <https://www.mdpi.com/article/10.3390/nanomanufacturing4030010/s1>, Figure S1: FTIR plots of (left row of graphs): untreated and coated with CV films, (a) un-LDPE_CV, (c) un-LDPE/10HNT_CV, (e) un-LDPE/10CV@HNT_CV, and of (right row of graphs) corona-treated and coated-with-CV films, (b) tr-LDPE_CV, (d) tr-LDPE/10HNT_CV, and (f) tr-LDPE/10CV@HNT_CV, on day 1, day 2, day 3, day 4, day 7, day 9, day 11, and day 14; Table S1: Calculated Young's Modulus (E), ultimate strength (σ_{uts}), and %elongation at break mean values along with the standard deviation values and statistical analysis results; Table S2: Calculated WVTR, D_{wv} , O.T.R., and Pe_{O_2} mean values along with the standard deviation values and statistical analysis results for all tested films. Table S3: Calculated %wt. CV release content (%RC_{CV}) as well as the CV release rate (RR_{CV}) mean values for all corona-treated and untreated active films. Table S4: Calculated EC₅₀ mean values along with standard deviation values and statistical analysis results for all tested films.

Author Contributions: Conceptualization, A.E.G., C.P. and C.E.S.; Data curation, V.K.K., A.D., A.A.L., M.A.K. and C.P.; Formal analysis, A.E.G., A.A.L., K.K., C.P. and C.E.S.; Investigation, A.E.G., V.K.K., A.N., A.D., A.A.L., K.K., M.A.K., C.P. and C.E.S.; Methodology, A.E.G., M.A.K., C.P. and C.E.S.; Project administration, A.E.G. and C.E.S.; Resources, A.E.G. and C.E.S.; Software, C.E.S.; Supervision, A.E.G. and C.E.S.; Validation, A.E.G. and C.E.S.; Visualization, A.E.G. and C.E.S.; Writing—original draft, A.E.G. and C.E.S.; Writing—review and editing, A.E.G. and C.E.S. All authors have read and agreed to the published version of the manuscript.

Funding: This research received no external funding.

Data Availability Statement: The datasets generated for this study are available on request to the corresponding author.

Conflicts of Interest: The authors declare no conflicts of interest.

References

1. Scarano, P.; Sciarrillo, R.; Tartaglia, M.; Zuzolo, D.; Guarino, C. Circular Economy and Secondary Raw Materials from Fruits as Sustainable Source for Recovery and Reuse. A Review. *Trends Food Sci. Technol.* **2022**, *122*, 157–170. [[CrossRef](#)]
2. Giannakas, A.E. Plant Extracts-Based Food Packaging Films. In *Plant Extracts-Based Food Packaging Films—Natural Materials for Food Packaging Application*; Wiley Online Library: Hoboken, NJ, USA, 2023; pp. 23–49. [[CrossRef](#)]
3. Hamam, M.; Chinnici, G.; Di Vita, G.; Pappalardo, G.; Pecorino, B.; Maesano, G.; D'Amico, M. Circular Economy Models in Agro-Food Systems: A Review. *Sustainability* **2021**, *13*, 3453. [[CrossRef](#)]
4. Carpena, M.; Nuñez-Estevez, B.; Soria-Lopez, A.; Garcia-Oliveira, P.; Prieto, M.A. Essential Oils and Their Application on Active Packaging Systems: A Review. *Resources* **2021**, *10*, 7. [[CrossRef](#)]
5. Chacha, J.S.; Ofoedu, C.E.; Xiao, K. Essential Oil-Based Active Polymer-Based Packaging System: A Review of Its Effect on the Antimicrobial, Antioxidant, and Sensory Properties of Beef and Chicken Meat. *J. Food Process. Preserv.* **2022**, *46*, e16933. [[CrossRef](#)]
6. Sánchez-González, L.; Vargas, M.; González-Martínez, C.; Chiralt, A.; Chafer, M. Use of Essential Oils in Bioactive Edible Coatings: A Review. *Food Eng. Rev.* **2011**, *3*, 1–16. [[CrossRef](#)]
7. Busolo, M.A.; Lagaron, J.M. Antioxidant Polyethylene Films Based on a Resveratrol Containing Clay of Interest in Food Packaging Applications. *Food Packag. Shelf Life* **2015**, *6*, 30–41. [[CrossRef](#)]
8. Coelho, L.B.; Geraldine, R.M.; Silveira, M.F.A.; de Souza, A.R.M.; Torres, M.C.L.; Gonçalves, M.Á.B. Characterization of Films of Low Density Polyethylene Incorporated with Oregano Essential Oil. *Res. Soc. Dev.* **2020**, *9*, e3849108722. [[CrossRef](#)]
9. de Araújo, L.O.; Anaya, K.; Pergher, S.B.C. Synthesis of Antimicrobial Films Based on Low-Density Polyethylene (LDPE) and Zeolite A Containing Silver. *Coatings* **2019**, *9*, 786. [[CrossRef](#)]
10. Farghal, H.H.; Karabagias, I.; El Sayed, M.; Kontominas, M.G. Determination of Antioxidant Activity of Surface-Treated PET Films Coated with Rosemary and Clove Extracts. *Packag. Technol. Sci.* **2017**, *30*, 799–808. [[CrossRef](#)]
11. Giannakas, A.E.; Salmas, C.E.; Karydis-Messinis, A.; Moschovas, D.; Kollia, E.; Tsigkou, V.; Proestos, C.; Avgeropoulos, A.; Zafeiropoulos, N.E. Nanoclay and Polystyrene Type Efficiency on the Development of Polystyrene/Montmorillonite/Oregano Oil Antioxidant Active Packaging Nanocomposite Films. *Appl. Sci.* **2021**, *11*, 9364. [[CrossRef](#)]
12. Aitboulahsen, M.; El Galiou, O.; Laglaoui, A.; Bakkali, M.; Hassani Zerrouk, M. Effect of Plasticizer Type and Essential Oils on Mechanical, Physicochemical, and Antimicrobial Characteristics of Gelatin, Starch, and Pectin-Based Films. *J. Food Process. Preserv.* **2020**, *44*, e14480. [[CrossRef](#)]
13. Souza, A.G.; Ferreira, R.R.; Paula, L.C.; Mitra, S.K.; Rosa, D.S. Starch-Based Films Enriched with Nanocellulose-Stabilized Pickering Emulsions Containing Different Essential Oils for Possible Applications in Food Packaging. *Food Packag. Shelf Life* **2021**, *27*, 100615. [[CrossRef](#)]
14. Abdollahi, M.; Rezaei, M.; Farzi, G. A Novel Active Bionanocomposite Film Incorporating Rosemary Essential Oil and Nanoclay into Chitosan. *J. Food Eng.* **2012**, *111*, 343–350. [[CrossRef](#)]
15. Almeida, R.R.; Silva Damasceno, E.T.; de Carvalho, S.Y.B.; de Carvalho, G.S.G.; Gontijo, L.A.P.; de Lima Guimarães, L.G. Chitosan Nanogels Condensed to Ferulic Acid for the Essential Oil of Lippia Origanoides Kunth Encapsulation. *Carbohydr. Polym.* **2018**, *188*, 268–275. [[CrossRef](#)]
16. Hasani, S.; Ojagh, S.M.; Ghorbani, M. Nanoencapsulation of Lemon Essential Oil in Chitosan-Hicap System. Part 1: Study on Its Physical and Structural Characteristics. *Int. J. Biol. Macromol.* **2018**, *115*, 143–151. [[CrossRef](#)]
17. Jiang, J.; Watowita, P.S.M.S.L.; Chen, R.; Shi, Y.; Geng, J.-T.; Takahashi, K.; Li, L.; Osako, K. Multilayer Gelatin/Myofibrillar Films Containing Clove Essential Oil: Properties, Protein-Phenolic Interactions, and Migration of Active Compounds. *Food Packag. Shelf Life* **2022**, *32*, 100842. [[CrossRef](#)]
18. Fiore, A.; Park, S.; Volpe, S.; Torrieri, E.; Masi, P. Active Packaging Based on PLA and Chitosan-Caseinate Enriched Rosemary Essential Oil Coating for Fresh Minced Chicken Breast Application. *Food Packag. Shelf Life* **2021**, *29*, 100708. [[CrossRef](#)]
19. Wongphan, P.; Nampanya, P.; Chakpha, W.; Promhuad, K.; Laurenza, Y.; Leelaphiwat, P.; Bumbudsanpharoke, N.; Sodsai, J.; Lorenzo, J.M.; Harnkarnsujarit, N. Lesser Galangal (*Alpinia officinarum* Hance) Essential Oil Incorporated Biodegradable PLA/PBS Films as Shelf-Life Extension Packaging of Cooked Rice. *Food Packag. Shelf Life* **2023**, *37*, 101077. [[CrossRef](#)]
20. Louis, E.; Villalobos-Carvajal, R.; Reyes-Parra, J.; Jara-Quijada, E.; Ruiz, C.; Andrades, P.; Gacitúa, J.; Beldarraín-Iznaga, T. Preservation of Mushrooms (*Agaricus bisporus*) by an Alginate-Based-Coating Containing a Cinnamaldehyde Essential Oil Nanoemulsion. *Food Packag. Shelf Life* **2021**, *28*, 100662. [[CrossRef](#)]
21. Arrieta, M.P.; López, J.; Ferrándiz, S.; Peltzer, M.A. Characterization of PLA-Limonene Blends for Food Packaging Applications. *Polym. Test.* **2013**, *32*, 760–768. [[CrossRef](#)]
22. Darvish, M.; Aji, A. Synergistic Antimicrobial Activities of Limonene with Mineral Carriers in LDPE Films for Active Packaging Application. *Sci. J. Chem.* **2022**, *10*, 32. [[CrossRef](#)]
23. Huang, X.; Ge, X.; Zhou, L.; Wang, Y. Eugenol Embedded Zein and Poly(Lactic Acid) Film as Active Food Packaging: Formation, Characterization, and Antimicrobial Effects. *Food Chem.* **2022**, *384*, 132482. [[CrossRef](#)]
24. Srisa, A.; Harnkarnsujarit, N. Antifungal Films from Trans-Cinnamaldehyde Incorporated Poly(Lactic Acid) and Poly(Butylene Adipate-Co-Terephthalate) for Bread Packaging. *Food Chem.* **2020**, *333*, 127537. [[CrossRef](#)]

25. Gámez, E.; Elizondo-Castillo, H.; Tascon, J.; García-Salinas, S.; Navascues, N.; Mendoza, G.; Arruebo, M.; Irusta, S. Antibacterial Effect of Thymol Loaded SBA-15 Nanorods Incorporated in PCL Electrospun Fibers. *Nanomaterials* **2020**, *10*, 616. [[CrossRef](#)]
26. Ochoa-Velasco, C.E.; Pérez-Pérez, J.C.; Varillas-Torres, J.M.; Navarro-Cruz, A.R.; Hernández-Carranza, P.; Munguía-Pérez, R.; Cid-Pérez, T.S.; Avila-Sosa, R. Starch Edible Films/Coatings Added with Carvacrol and Thymol: In Vitro and In Vivo Evaluation against *Colletotrichum Gloeosporioides*. *Foods* **2021**, *10*, 175. [[CrossRef](#)]
27. Pei, R.S.; Zhou, F.; Ji, B.P.; Xu, J. Evaluation of Combined Antibacterial Effects of Eugenol, Cinnamaldehyde, Thymol, and Carvacrol against *E. coli* with an Improved Method. *J. Food Sci.* **2009**, *74*, 379–383. [[CrossRef](#)]
28. Babayev, A.; Spasojević, L.; Škrbić, J.; Bučko, S.; Kocić-Tanackov, S.; Bulut, S.; Fraj, J.; Petrović, L.; Milinković Budinčić, J.; Sharipova, A.; et al. Antimicrobial Pseudolatex Zein Films with Encapsulated Carvacrol for Sustainable Food Packaging. *Food Packag. Shelf Life* **2023**, *37*, 101076. [[CrossRef](#)]
29. Sakkas, H.; Papadopoulou, C. Antimicrobial Activity of Basil, Oregano, and Thyme Essential Oils. *J. Microbiol. Biotechnol.* **2017**, *27*, 429–438. [[CrossRef](#)]
30. Mehalaine, S.; Belfadel, O.; Menasria, T.; Messaili, A. Chemical Composition and Antibacterial Activity of Essential Oils of Three Medicinal Plants from Algerian Semi-Arid Climatic Zone. *Phytothérapie* **2017**, *15*, 1–9. [[CrossRef](#)]
31. Sharifi-Rad, M.; Varoni, E.M.; Iriti, M.; Martorell, M.; Setzer, W.N.; Del Mar Contreras, M.; Salehi, B.; Soltani-Nejad, A.; Rajabi, S.; Tajbakhsh, M.; et al. Carvacrol and Human Health: A Comprehensive Review. *Phytother. Res.* **2018**, *32*, 1675–1687. [[CrossRef](#)]
32. Li, Q.; Ren, T.; Perkins, P.; Hu, X.; Wang, X. Applications of Halloysite Nanotubes in Food Packaging for Improving Film Performance and Food Preservation. *Food Control.* **2021**, *124*, 107876. [[CrossRef](#)]
33. de Oliveira, L.H.; Trigueiro, P.; Souza, J.S.N.; de Carvalho, M.S.; Osajima, J.A.; da Silva-Filho, E.C.; Fonseca, M.G. Montmorillonite with Essential Oils as Antimicrobial Agents, Packaging, Repellents, and Insecticides: An Overview. *Colloids Surf. B Biointerfaces* **2022**, *209*, 112186. [[CrossRef](#)]
34. Mitura, K.; Kornacka, J.; Kopczyńska, E.; Kalisz, J.; Czerwińska, E.; Affeltowicz, M.; Kaczorowski, W.; Kolesińska, B.; Frączyk, J.; Bakalova, T.; et al. Active Carbon-Based Nanomaterials in Food Packaging. *Coatings* **2021**, *11*, 161. [[CrossRef](#)]
35. Villa, C.C.; Valencia, G.A.; López Córdoba, A.; Ortega-Toro, R.; Ahmed, S.; Gutiérrez, T.J. Zeolites for Food Applications: A Review. *Food Biosci.* **2022**, *46*, 101577. [[CrossRef](#)]
36. Videira-Quintela, D.; Martin, O.; Montalvo, G. Emerging Opportunities of Silica-Based Materials within the Food Industry. *Microchem. J.* **2021**, *167*, 106318. [[CrossRef](#)]
37. Kurd, F.; Fathi, M.; Shekarchizadeh, H. Basil Seed Mucilage as a New Source for Electrospinning: Production and Physicochemical Characterization. *Int. J. Biol. Macromol.* **2017**, *95*, 689–695. [[CrossRef](#)]
38. Suppakul, P.; Miltz, J.; Sonneveld, K.; Bigger, S.W. Active Packaging Technologies with an Emphasis on Antimicrobial Packaging and Its Applications. *J. Food Sci.* **2003**, *68*, 408–420. [[CrossRef](#)]
39. Andrade, M.A.; Barbosa, C.H.; Souza, V.G.L.; Coelho, I.M.; Reboleira, J.; Bernardino, S.; Ganhão, R.; Mendes, S.; Fernando, A.L.; Vilarinho, F.; et al. Novel Active Food Packaging Films Based on Whey Protein Incorporated with Seaweed Extract: Development, Characterization, and Application in Fresh Poultry Meat. *Coatings* **2021**, *11*, 229. [[CrossRef](#)]
40. Gaikwad, K.K.; Singh, S.; Lee, Y.S. A Pyrogallol-Coated Modified LDPE Film as an Oxygen Scavenging Film for Active Packaging Materials. *Prog. Org. Coat.* **2017**, *111*, 186–195. [[CrossRef](#)]
41. Fu, Y.; Dudley, E.G. Antimicrobial-Coated Films as Food Packaging: A Review. *Compr. Rev. Food Sci. Food Saf.* **2021**, *20*, 3404–3437. [[CrossRef](#)]
42. Tyuftin, A.A.; Kerry, J.P. Review of Surface Treatment Methods for Polyamide Films for Potential Application as Smart Packaging Materials: Surface Structure, Antimicrobial and Spectral Properties. *Food Packag. Shelf Life* **2020**, *24*, 100475. [[CrossRef](#)]
43. Louzi, V.C.; Campos, J.S.D.C. Corona Treatment Applied to Synthetic Polymeric Monofilaments (PP, PET, and PA-6). *Surf. Interfaces* **2019**, *14*, 98–107. [[CrossRef](#)]
44. Dai, L.; Xu, D. Polyethylene Surface Enhancement by Corona and Chemical Co-Treatment. *Tetrahedron Lett.* **2019**, *60*, 1005–1010. [[CrossRef](#)]
45. Božović, A.; Tomašević, K.; Benbettaieb, N.; Debeaufort, F. Influence of Surface Corona Discharge Process on Functional and Antioxidant Properties of Bio-Active Coating Applied onto PLA Films. *Antioxidants* **2023**, *12*, 859. [[CrossRef](#)] [[PubMed](#)]
46. Giannakas, A.E.; Salmas, C.E.; Moschovas, D.; Zaharioudakis, K.; Georgopoulos, S.; Asimakopoulos, G.; Aktypis, A.; Proestos, C.; Karakassides, A.; Avgeropoulos, A.; et al. The Increase of Soft Cheese Shelf-Life Packaged with Edible Films Based on Novel Hybrid Nanostructures. *Gels* **2022**, *8*, 539. [[CrossRef](#)] [[PubMed](#)]
47. Giannakas, A.E.; Salmas, C.E.; Moschovas, D.; Karabagias, V.K.; Karabagias, I.K.; Baikousi, M.; Georgopoulos, S.; Leontiou, A.; Katerinopoulou, K.; Zafeiropoulos, N.E.; et al. Development, Characterization, and Evaluation as Food Active Packaging of Low-Density-Polyethylene-Based Films Incorporated with Rich in Thymol Halloysite Nanohybrid for Fresh “Scaloppini” Type Pork Meat Fillets Preservation. *Polymers* **2023**, *15*, 282. [[CrossRef](#)] [[PubMed](#)]
48. Giannakas, A.E.; Karabagias, V.K.; Moschovas, D.; Leontiou, A.; Karabagias, I.K.; Georgopoulos, S.; Karydis-Messinis, A.; Zaharioudakis, K.; Andritsos, N.; Kehayias, G.; et al. Thymol@activated Carbon Nanohybrid for Low-Density Polyethylene-Based Active Packaging Films for Pork Fillets’ Shelf-Life Extension. *Foods* **2023**, *12*, 2590. [[CrossRef](#)] [[PubMed](#)]
49. Salmas, C.E.; Giannakas, A.E.; Karabagias, V.K.; Moschovas, D.; Karabagias, I.K.; Gioti, C.; Georgopoulos, S.; Leontiou, A.; Kehayias, G.; Avgeropoulos, A.; et al. Development and Evaluation of a Novel-Thymol@Natural-Zeolite/Low-Density-Polyethylene Active Packaging Film: Applications for Pork Fillets Preservation. *Antioxidants* **2023**, *12*, 523. [[CrossRef](#)] [[PubMed](#)]

50. Karabagias, V.K.; Giannakas, A.E.; Andritsos, N.D.; Leontiou, A.A.; Moschovas, D.; Karydis-Messinis, A.; Avgeropoulos, A.; Zafeiropoulos, N.E.; Proestos, C.; Salmas, C.E. Shelf Life of Minced Pork in Vacuum-Adsorbed Carvacrol@Natural Zeolite Nanohybrids and Poly-Lactic Acid/Triethyl Citrate/Carvacrol@Natural Zeolite Self-Healable Active Packaging Films. *Antioxidants* **2024**, *13*, 776. [[CrossRef](#)]
51. Salmas, C.E.; Kollia, E.; Avdylaj, L.; Kopsacheili, A.; Zaharioudakis, K.; Georgopoulos, S.; Leontiou, A.; Katerinopoulou, K.; Kehayias, G.; Karakassides, A.; et al. Thymol@Natural Zeolite Nanohybrids for Chitosan/Poly-Vinyl-Alcohol Based Hydrogels Applied As Active Pads. *Gels* **2023**, *9*, 570.
52. Lahti, J. The Effects of Corona and Flame Treatment: Part 1. PE-LD Coated Packaging Board. In Proceedings of the 11th TAPPI Europlace Conference, Athens, Greece, 14–16 May 2007.
53. Salmas, C.E.; Giannakas, A.E.; Baikousi, M.; Kollia, E.; Tsigkou, V.; Proestos, C. Effect of Copper and Titanium-Exchanged Montmorillonite Nanostructures on the Packaging Performance of Chitosan/Poly-Vinyl-Alcohol-Based Active Packaging Nanocomposite Films. *Foods* **2021**, *10*, 3038. [[CrossRef](#)]
54. Brand-Williams, W.; Cuvelier, M.E.; Berset, C. Use of a Free Radical Method to Evaluate Antioxidant Activity. *LWT Food Sci. Technol.* **1995**, *28*, 25–30. [[CrossRef](#)]
55. Karabagias, I.K.; Maia, M.; Karabagias, V.K.; Gatzias, I.; Badeka, A.V. Characterization of Eucalyptus, Chestnut and Heather Honeys from Portugal Using Multi-Parameter Analysis and Chemo-Calculus. *Foods* **2018**, *7*, 194. [[CrossRef](#)]
56. Sadeq, T.W.; Kamel, F.H.; Qader, K.O. A Novel Preparation of Thyme Cream as Superficial Antimicrobial Treatment. *J. Int. Pharm. Res.* **2019**, *46*, 373–381.
57. Valderrama, A.C.S.; Rojas, G.C.R.D. Traceability of Active Compounds of Essential Oils in Antimicrobial Food Packaging Using a Chemometric Method by ATR-FTIR. *Am. J. Anal. Chem.* **2017**, *8*, 726–741. [[CrossRef](#)]
58. Salmas, C.E.; Giannakas, A.E.; Moschovas, D.; Kollia, E.; Georgopoulos, S.; Gioti, C.; Leontiou, A.; Avgeropoulos, A.; Kopsacheili, A.; Avdylaj, L.; et al. Kiwi Fruits Preservation Using Novel Edible Active Coatings Based on Rich in Thymol Halloysite Nanostructures and Chitosan/Polyvinyl Alcohol Gels. *Gels* **2022**, *8*, 823. [[CrossRef](#)]
59. Li, H.; Zhu, X.; Zhou, H.; Zhong, S. Functionalization of Halloysite Nanotubes by Enlargement and Hydrophobicity for Sustained Release of Analgesic. *Colloids Surf. A Physicochem. Eng. Asp.* **2015**, *487*, 154–161. [[CrossRef](#)]
60. Martínez-Camacho, A.P.; Cortez-Rocha, M.O.; Graciano-Verdugo, A.Z.; Rodríguez-Félix, F.; Castillo-Ortega, M.M.; Burgos-Hernández, A.; Ezquerro-Brauer, J.M.; Plascencia-Jatomea, M. Extruded Films of Blended Chitosan, Low Density Polyethylene and Ethylene Acrylic Acid. *Carbohydr. Polym.* **2013**, *91*, 666–674. [[CrossRef](#)]
61. Giannakas, A.; Salmas, C.; Leontiou, A.; Tsimogiannis, D.; Oreopoulou, A.; Braouhli, J. Novel LDPE/Chitosan Rosemary and Melissa Extract Nanostructured Active Packaging Films. *Nanomaterials* **2019**, *9*, 1105. [[CrossRef](#)]
62. Giannakas, A.E.; Salmas, C.E.; Leontiou, A.; Baikousi, M.; Moschovas, D.; Asimakopoulos, G.; Zafeiropoulos, N.E.; Avgeropoulos, A. Synthesis of a Novel Chitosan/Basil Oil Blend and Development of Novel Low Density Poly Ethylene/Chitosan/Basil Oil Active Packaging Films Following a Melt-Extrusion Process for Enhancing Chicken Breast Fillets Shelf-Life. *Molecules* **2021**, *26*, 1585. [[CrossRef](#)]
63. Ornelas-Paz, J.D.J.; Zamudio-Flores, P.B.; Torres-Cisneros, C.G.; Holguín-Soto, R.; Ramos-Aguilar, O.P.; Ruiz-Cruz, S.; Guevara-Arauz, J.C.; González-Aguilar, G.A.; Santana-Rodríguez, V. The Barrier Properties and Potential Use of Recycled-LDPE Films as a Packaging Material to Preserve the Quality of Jalapeño Peppers by Modified Atmospheres. *Sci. Hortic.* **2012**, *135*, 210–218. [[CrossRef](#)]
64. Shemesh, R.; Krepker, M.; Natan, M.; Danin-Poleg, Y.; Banin, E.; Kashi, Y.; Nitzan, N.; Vaxman, A.; Segal, E. Novel LDPE/Halloysite Nanotube Films with Sustained Carvacrol Release for Broad-Spectrum Antimicrobial Activity. *RSC Adv.* **2015**, *5*, 87108–87117. [[CrossRef](#)]
65. Riyandari, B.A.; Suherman, S.; Siswanta, D. The Physico-Mechanical Properties and Release Kinetics of Eugenol in Chitosan-Alginate Polyelectrolyte Complex Films as Active Food Packaging. *Indones. J. Chem.* **2018**, *18*, 82–91. [[CrossRef](#)]
66. Dhoot, G.; Auras, R.; Rubino, M.; Dolan, K.; Soto-Valdez, H. Determination of Eugenol Diffusion through LLDPE Using FTIR-ATR Flow Cell and HPLC Techniques. *Polymer* **2009**, *50*, 1470–1482. [[CrossRef](#)]
67. Munteanu, B.S.; Sacarescu, L.; Vasiliu, A.-L.; Hitruc, G.E.; Pricope, G.M.; Sivertsvik, M.; Rosnes, J.T.; Vasile, C. Antioxidant/Antibacterial Electrospun Nanocoatings Applied onto PLA Films. *Materials* **2018**, *11*, 1973. [[CrossRef](#)]
68. Cox, H.J.; Sharples, G.J.; Badyal, J.P.S. Tea-Essential Oil-Metal Hybrid Nanocoatings for Bacterial and Viral Inactivation. *ACS Appl. Nano Mater.* **2021**, *4*, 12619–12628. [[CrossRef](#)]

Disclaimer/Publisher’s Note: The statements, opinions and data contained in all publications are solely those of the individual author(s) and contributor(s) and not of MDPI and/or the editor(s). MDPI and/or the editor(s) disclaim responsibility for any injury to people or property resulting from any ideas, methods, instructions or products referred to in the content.